Unveiling Hidden DNN Defects with Decision-Based Metamorphic Testing

Yuanyuan Yuan
The Hong Kong University of Science and Technology
Hong Kong, China
yyuanaq@cse.ust.hk

Qi Pang
The Hong Kong University of Science and Technology
Hong Kong, China
qpangaa@cse.ust.hk

Shuai Wang*
The Hong Kong University of Science and Technology
Hong Kong, China
shuaiw@cse.ust.hk

Abstract

Contemporary DNN testing works are frequently conducted using metamorphic testing (MT). In general, de facto MT frameworks mutate DNN input images using semantics-preserving mutations and determine if DNNs can yield consistent predictions. Nevertheless, we find that DNNs may *rely on erroneous decisions (certain components on the DNN inputs) to make predictions*, which may still retain the outputs by chance. Such DNN defects would be neglected by existing MT frameworks. Erroneous decisions, however, would likely result in successive mis-predictions over diverse images that may exist in real-life scenarios.

This research aims to unveil the pervasiveness of hidden DNN defects caused by incorrect DNN decisions (but retaining consistent DNN predictions). To do so, we tailor and optimize modern eXplainable AI (XAI) techniques to identify visual concepts that represent regions in an input image upon which the DNN makes predictions. Then, we extend existing MT-based DNN testing frameworks to check the *consistency of DNN decisions* made over a test input and its mutated inputs. Our evaluation shows that existing MT frameworks are oblivious to a considerable number of DNN defects caused by erroneous decisions. We conduct human evaluations to justify the validity of our findings and to elucidate their characteristics. Through the lens of DNN decision-based metamorphic relations, we re-examine the effectiveness of metamorphic transformations proposed by existing MT frameworks. We summarize lessons from this study, which can provide insights and guidelines for future DNN testing.

CCS Concepts

• **Software and its engineering** → *Software testing and debugging*.

Keywords

Deep learning testing

*Corresponding Author

ASE '22, October 10–14, 2022, Rochester, MI, USA

ACM ISBN 978-1-4503-9475-8/22/10…$15.00
https://doi.org/10.1145/3551349.3561157

ACM Reference Format:
Yuanyuan Yuan, Qi Pang, and Shuai Wang. 2022. Unveiling Hidden DNN Defects with Decision-Based Metamorphic Testing. In *37th IEEE/ACM International Conference on Automated Software Engineering (ASE '22), October 10–14, 2022, Rochester, MI, USA.* ACM, New York, NY, USA, 13 pages. https://doi.org/10.1145/3551349.3561157

1 Introduction

Metamorphic testing (MT) [7] has achieved a major success to comprehensively test deep neural networks (DNNs) without manually annotating test inputs [36]. Given the inherent difficulty of defining explicit testing oracles for DNN models [67], DNN is often tested using well-designed metamorphic relations (MRs): DNN inputs are mutated into new test cases in a semantics-preserving manner[1], and DNN predictions over an input and its mutated inputs are compared for consistency. DNN defects are characterized as violations of DNN prediction consistency. However, despite the major success of checking prediction consistency, we pose the following key question to motivate this research:

> "*Is it always the case that a consistent prediction indicates no DNN defect?*"

In this research, we refer to the DNN's focus on critical input components as its *decisions*. Accordingly, DNN relies on such decisions to make *predictions* (i.e., its outputs), e.g., classifying an input image. Then, consider Fig. 1, in which we illustrate how a contemporary MT framework misses a DNN defect. The tested DNN predicts "hummingbird" for Fig. 1(a), and its utilized decisions in Fig. 1(a) are marked in Fig. 1(b), depicting the correct scope of a hummingbird's head and body. When Fig. 1(a) is rotated as in Fig. 1(c), the DNN still predicts "hummingbird." Thus, existing MRs based on DNN output consistency would regard the DNN as "correct" for this case. Nevertheless, as in Fig. 1(d), the underlying DNN decision is *specious*, as it is based on a flower whose contour is similar to the contour of the flying hummingbird in Fig. 1(b).

(a) hummingbird image (b) decision based on hummingbird (c) rotated image (d) incorrect decision

Figure 1: DNN is making inconsistent, erroneous decisions while happening to retain the same prediction. We simplify the decision regions for readability.

[1]In this paper, semantics-preserving denotes that the contents in inputs and mutated inputs are visually consistent, e.g., a cat is still a cat.

Our preliminary study shows that existing MT-based DNN testing frameworks, when only checking the consistency of DNN predictions, may overlook DNN defects due to incorrect DNN decisions, i.e., relying on specious components in the DNN inputs for predictions. As revealed in this research, such incorrect decisions do not always result in inconsistent DNN outputs, especially when the DNN is trained on a dataset with limited labels (e.g., two-label classification), because DNN prediction is forced to choose among pre-defined labels. Consider a DNN ϕ that is trained on evenly distributed data and is performing a two-class (cat vs. dog) classification task. Assume that when random noise is applied to an image i, ϕ ignores the cat in i and randomly guesses a label. That is, it still has a 50% chance of predicting the correct label. Despite the fact that the tested DNN is flawed, it is nonetheless considered as "robust to noise" in many of these cases.

Moreover, we clarify that specious DNN decisions are hard to detect using only the DNN predictions and confidence scores. A well-trained DNN predicts a pre-defined label with a confidence score that is typically much higher than the other labels, even when given random noise as inputs. Thus, even if DNN is generating erroneous decisions, its outputs and accompanying confidence scores often lack an evident "pattern." This difficulty is also highlighted in prior literatures [22, 43].

Overall, this work deems inconsistent DNN decisions exposed by MT are specious and undesirable, as it is likely that a DNN, even if it happens to correctly label an image (Fig. 1(c)), will eventually mis-predict a hummingbird for pervasive images existing in real-world scenarios. As a result, we argue that failing to account for DNN decision defects may jeopardize the reliability of present MT frameworks. We advocate that *proper MRs should take DNN decisions into consideration, rather than merely checking DNN predictions.*

This work advocates to extend DNN prediction-based consistency checking, which is extensively used in current MT, with decision-based consistency checking. The enhancement is orthogonal to particular metamorphic transformations (e.g., image pixel or affine transformations) implemented in existing MT-based DNN testing frameworks, and can be smoothly incorporated by them. Given an test image i, we extract the decision, denoting regions in i, to depict how DNN makes prediction over i. Each region is referred to as a visual concept (e.g., a nose or a wheel), and DNN predictions can be formulated as a voting scheme among visual concepts [18, 34]. To obtain visual concepts, we first use eXplainable AI (XAI) techniques to identify pixels in i that positively contribute to the DNN prediction. Then, we tailor and optimize a set of image processing techniques to construct visual concepts from XAI-identified pixels. We carefully reduce inherent inaccuracy of XAI techniques, and largely enhance the readability of identified visual concepts.

By extending existing MT frameworks to support decision-based consistency checking, we uncover many overlooked defects triggered by inputs that result in inconsistent decisions but identical predictions. Our findings are justified by large-scale and comprehensive (in total 10,000) human evaluations, where the participants are 15 Ph.D. students having research experiences related to DNNs and 10 other Ph.D. and masters students of various backgrounds. Our study encompasses ten DNNs over three datasets of different scales and types (e.g., RGB and black-white images) which are all popular in daily usage and have been extensively tested by previous DNN testing research. We summarize key lessons of this research, illustrating that existing MT, when only checking DNN prediction consistency, may over-estimate the reliability of DNNs. We also assess the strength of metamorphic transformations (e.g., pixel mutation vs. adversarial perturbation) proposed by existing work through the lens of our novel DNN decision view. Our findings and summarized lessons can provide insights for follow-up enhancement of DNN testing. In sum, we make the following contributions.

- We advocate that existing MT-based DNN testing should consider how DNN makes decisions rather than merely checking predictions. Accordingly, we extend existing MRs by checking decision consistency to reveal DNN defects overlooked by existing works.
- Technically, we recast a DNN prediction as the outcome of a voting process among visual concepts in an input. We tailor and optimize image processing schemes to summarize visual concepts from image pixels positively contributing DNN predictions.
- Our study and human evaluation illustrate that many defects have been overlooked when only checking DNN prediction consistency. Our findings provide guidelines for users to calibrate MT-based DNN testing results, and also highlight further improvements that can be made by DNN testing.

To support results verification and follow-up research comparison, we released code, data, and supplementary materials at [1].

2 Preliminary and Motivation

2.1 Metamorphic Testing

DNNs are typically used to answer unknown questions where they are anticipated to behave similarly to humans [67]. Given the diversity of possible inputs encountered in real-life scenarios, obtaining ground truth predictions in advance to assess DNN correctness is difficult, if not impossible. Furthermore, even human experts may disagree on expected outputs of certain edge cases.

MT is extensively employed to test DNNs without the need for ground-truth or explicitly defined testing oracles [7]. Overall, each MR in MT composes a metamorphic transformation MR_t and a relation MR_r: each MR_t specifies a mutation scheme over a source input to generate a follow-up test input, and the associated MR_r defines the relationship of expected outputs over the source and the mutated input [49]. For instance, to test $sin(x)$, we can construct an MR such that its MR_t mutates an input x into $\pi - x$, and the MR_r checks the the equality relation $sin(x) = sin(\pi - x)$. In real-world usage, MR_r usually denotes invariant program properties. MR_r should always hold when arbitrarily mutating x using MR_t, and a bug in $sin(x)$ is detected whenever MR_r is violated.

MT achieves major success in testing DNN models and infrastructures [10, 13, 14, 33, 37, 38, 42, 59, 62–66, 68]. Given DNN inputs are often images, MRs in this field are often constructed to perform lightweight, semantics-preserving (visually consistent) image mutations MR_t from different angles (see Sec. 5 for MR_t designed in previous works). MR_r is defined in a simple and unified manner such that DNN predictions should be *consistent* over an input image and its follow-up image generated by using MR_t. Thus, violation of MR_r, denoting inconsistent DNN predictions, are DNN defects.

Table 1: Four MR_r based on DNN decisions (D_1, D_2) and predictions (L_1, L_2) over an input and its mutated input.

	①$D_1 = D_2$ $L_1 = L_2$	②$D_1 \neq D_2$ $L_1 \neq L_2$	③$D_1 \neq D_2$ $L_1 = L_2$	④$D_1 = D_2$ $L_1 \neq L_2$
No defect?	✓	✗	✗	NA

2.2 Forming MR_r with DNN Decisions

Without knowledge of a DNN's decision procedure, we argue that relying merely on its output (as how existing MR_r is formed) may result in the omission of some defects. Given a pair of inputs i_1 and i_2 (i_2 is mutated from i_1 using a MR_t), suppose the DNN yields prediction L_1 based on decision D_1, yielding L_2 based on decision D_2.[2] Then, we have four combinations of decisions/predictions, as in Table 1. ① denotes a correct prediction (from the perspective of MT), whereas ② represents that the DNN provides inconsistent predictions $L1 \neq L2$. As introduced in Sec. 2.1, existing MT frameworks rely on ② to form MR_r, and we clarify that ④ is not feasible: $D_1 = D_2 \rightsquigarrow L_1 \neq L_2$ violates the nature of a DNN.

We explore a new focus to form MR_r, as in ③, where DNNs make inconsistent decisions ($D_1 \neq D_2$), but still happen to retain the same prediction ($L_1 = L_2$). We deem them as *hidden DNN defects* that are incorrectly overlooked by existing works. Suppose a DNN ϕ answers if hummingbirds appear in an image. ϕ is trained on a biased dataset where all hummingbirds hover in the air, and therefore, ϕ wrongly relies on "vertical objects" to recognize hummingbird. For Fig. 1(a), it is properly predicted by ϕ as "yes" due to the hovering hummingbird. After rotating this image for 90 degrees as in Fig. 1(c), we find that ϕ still responds "yes," but makes decision based the vertically presented identified flower in Fig. 1(d), which shares a similar contour to most hummingbirds (e.g., by comparing with the contour in Fig. 1(b)). In fact, to ensure that identified DNN decisions are correct, we manually retain only the flower in Fig. 1(d) (by erasing the remaining components) and ϕ still predicts the image as a "hummingbird." Moreover, while ϕ is obviously susceptible to rotation, MR_r based on ② cannot uncover the defect. Nevertheless, this hidden flaw can be unveiled by MR_r based on ③.

Paper Structure. In the rest of this paper, we formulate D in Sec. 2.3, and present technical solutions to constitute D in Sec. 4. We review literatures of MT-based DNN testing and their proposed MR_t in Sec. 5. Sec. 6 unveils the pervasiveness of hidden defects falling in ③ with empirical results.

Incompaliance of Ground Truth. Following the notation above, let the ground truth prediction be L_G. It is widely seen that MT may result in false negatives due to $L_G \neq (L_1 = L_2)$. That is, a DNN makes consistent albeit incorrect predictions over i_1 and i_2. Similarly, let the ground truth decision be D_G, we clarify that false negatives may occur, in case $D_G \neq (D_1 = D_2)$. This may be due to the incorrect (albeit consistent) decisions made by a DNN, or the analysis errors of our employed XAI algorithms. Overall, MT inherently omits considering $D_G \neq (D_1 = D_2)$; detecting such flaws likely requires human annotations, which is highly costly in real-world settings. On the other hand, as empirically assessed in Sec. 6.1, D obtained in this work is accurate.

[2] D is formed by identifying DNN's decision over the input i; see Sec. 4 for details.

2.3 DNN Decision: A Pixel-Based View

We now introduce how a DNN makes decisions. Aligned with previous research, this paper primarily considers testing DNN image classifiers, and our following introduction uses image classification as an example accordingly. Many common DNN tasks root from an accurate image classification (see further discussion in Sec. 7). We first define the `Empty` and `Valid` inputs below.

Definition 1 (`Empty`). *An input is empty if its components are meaningless for humans, e.g., an image with random pixel values.*

Definition 2 (`Valid`). *An input is valid if its components are meaningful for humans, e.g., images of human-recognizable objects.*

Given an empty image $\emptyset$, a well-trained DNN ϕ will have to randomly predict a confidence score for each class and the score for class l is $\phi(\emptyset)^l$. A valid input image i can be viewed as introducing the appearances of its components by changing pixel values over $\emptyset$, namely, setting $i = \emptyset + \delta$. Accordingly, the output confidence score for class l is transformed into $\phi(i)^l = \phi(\emptyset)^l + \Delta^l$ given all these appearances in input. The machine learning community generally views this procedure as a collaborative game among pixels of i [2, 3, 9, 35, 41, 48, 53, 56]. The true contribution of each pixel can be computed via the Shapley value [51] — a well-established solution in game theory. We present how to use Shapley value to `attribute` Δ^l on δ below in Definition 3. We then discuss its approximation and present cost analysis.

Definition 3 (`Attribution`). *Let each pixel change be δ_p and $\sum \delta_p = \delta$. Then, an* `attribution` *of Δ^l assigns a contribution score c_p to each δ_p, such that $\sum c_p = \Delta^l$, where p represents one pixel.*

From Pixel-Wise Contributions to Decision D. A pixel p positively supports the DNN prediction for class l if its contribution $c_p > 0$. Therefore, collecting all pixels with positive contributions can help scoping the decision D upon which DNN ϕ relies when processing i and predicting l. Instead of using pixels, however, we abstract further to group pixels with positive contributions into visual concepts (e.g., a nose or a wheel) in i, and a DNN's predictions can be decomposed as a voting scheme among visual concepts. Each decision D comprises all of its visual concepts. We explain how visual concepts are generated among pixels in Sec. 2.4.

Approximating Shapley Value in XAI. As aforementioned, each pixel in an image is considered as a player in the collaborative game (i.e., making a prediction). Let all pixels in an image be $\mathbb{X}$, then calculating the exact Shapley value requires considering all subset of $\mathbb{X}$ which results in a computational cost of $2^{|\mathbb{X}|}$ and is infeasible in practice. Nevertheless, modern attribution-based XAI [35] have enabled practical approximation of Shapley value. In this research, we use DeepLIFT [53], a popular XAI tool, to identify pixels p in an image that positively contribute to the decision of a DNN. Though recent works may be able to identify more precise `attributions` than DeepLIFT, their computation is usually expensive [8, 35, 53]. Also, as noted in Sec. 4, DeepLIFT's potentially imprecise pixel-level attributions can be cleverly alleviated using our methods.

2.4 DNN Decision: A Visual Concept View

It is generally acknowledged that the visual concepts are the basic perception units captured by humans when perceiving the

(a) input image (b) "positive" pixels obtained via std. XAI (c) visual concepts

Figure 2: Pixels of positive contributions in standard XAI vs. visual concepts converted by our approach.

world [28, 40, 60]. For instance, a human may recognize a coucal based on its head and tail, as highlighted in Fig. 2(c), rather than those pixels marked in Fig. 2(b). We now define the visual concepts:

Definition 4 (Visual Concept). *A visual concept denotes a semantics meaningful instance on an image, e.g., wheels of a car, or a mark on a car. Generally, each visual concept is a connected non-trivial pixel-region and different visual concepts are disconnected.*

Advantage of Visual Concepts.[3] As clarified in Sec. 2.3, we use DeepLIFT, a popular XAI tool, to identify pixels in a DNN input that positively contribute to DNN predictions. Considering the image (a DNN input) in Fig. 2(a), we use DeepLIFT to identify pixels of positive contributions, as shown in Fig. 2(b). However, "positive" pixels span the entire image and their pixel-wise attribution is *too sensitive* to be used as a testing oracle — it is unclear if we have found a "defect" where only the contributions of a few pixels are flipped (e.g., from positively supporting to non-supporting). Moreover, XAI approaches are not always accurate, as this task is inherently challenging. In contrast, we abstract pixels into visual concepts for comparison (as in Fig. 2(c)), which are shown as more robust to potential inaccuracy of XAI, as trivial pixel-level changes are less likely to differ visual concepts. Moreover, while a single pixel is less interpretable for humans, visual concepts can explain DNN decisions (e.g., image classification) in a much more understandable manner; see the following discussion.

(a) ambulance image (b) decision for "ambulance" (c) incorrect decision

Figure 3: DNN Decision (based on visual concepts) for an ambulance image and the one with increased brightness.

Image Classification based on Visual Concepts. Visual concepts typically reflect DNN decisions in a human understandable manner. The prediction "ambulance" for Fig. 3(a) can be deconstructed into the visual concepts presented in Fig. 3(b), where the presence of `wheels` (visual concepts) enables the DNN to classify the image as car-like. The `siren` then reduces the possible categories to "police car" and "ambulance." The "ambulance" is confirmed according to the `cross mark`. The `wheels`, `siren`, and `cross mark` all support the prediction "ambulance" in this case. These three visual concepts

[3]The "visual concept", which denotes one region of an input image, is different with what defined in Activation Atlases [5] (i.e., one neuron output).

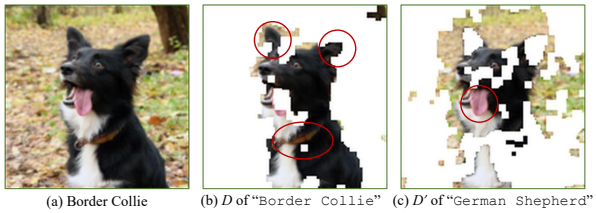

(a) Border Collie (b) D of "Border Collie" (c) D' of "German Shepherd"

Figure 4: Inconsistent D and D' when the DNN is making *inconsistent* predictions. Decision is marked.

(a) Thimble (b) D of "thimble" (c) D' of "thimble"

Figure 5: Inconsistent D and D' when the DNN is making an *identical* prediction. Decision is marked.

form the decision. In other words, the DNN is deemed to behave incorrectly if certain perturbations result in its decision-making based on distinct visual concepts. For instance, when the image brightness is increased (as in Fig. 3(c)), the DNN no longer relies on the `siren` and `cross mark` to make decisions. Despite the DNN still predicts "ambulance" (by randomly guessing within car-like categories), this is deemed a defect in this study.

Extracting Visual Concepts. As noted in Sec. 2.2, we employ XAI techniques to mark pixels in a test input that positively contribute to the DNN's prediction. We further customize and optimize image processing techniques to construct decision D over those pixels with positive contributions; see details in Sec. 4.1.

Comparison with Other Methods. Some works obtain DNN decisions without attribution, but instead use heatmaps whose application scope is *limited*. For example, the state-of-the-art approach Grad-CAM can fail if an image has multiple instances of the same classes [6, 50], which is prevalent in real images. In addition, other occlusion-based techniques involve removing/inserting an object to the input and observing if the prediction changed to decide decision [58, 62]. These approaches, however, require pre-defining and annotating instances in images, which may impede automated and comprehensive DNN testing. In contrast, *we generate visual concepts without human intervention, hence allowing an automated pipeline.* DNN decisions can also be assessed by observing the DNN internal activities. For instance, Wang et al. [61] dissect a DNN as multiple sub-models and evaluate the internal decision consistency to decide the prediction correctness. This work is orthogonal to our approach, as we focus on DNN inputs. Enhancing our approach with DNN internal activities is an interesting future work.

3 Approach Overview

By feeding a test image i to an DNN ϕ, we use $\phi[[i]].L$ to denote the prediction (i.e., labels), and $\phi[[i]].D$ to signify the decision; $\phi[[i]].D$ contains a set of visual concepts (fragments) on i that supports ϕ to yield $\phi[[i]].L$. As introduced in Sec. 2.2, this work aims to identify DNN defects that are omitted by existing MT frameworks using the MR:

$$\mathcal{E}_l(\mathcal{M}[[i]].L, \mathcal{M}[[i']].L) \wedge \mathcal{E}_d(\mathcal{M}[[i]].D, \mathcal{M}[[i']].D) \quad (1)$$

Mutating i into i'. Here, i' is mutated from a test image i using MR_t proposed by existing MT-based DNN testing works. For instance, MR_t can be pixel-wise transformations or affine transformations. See a full list of MR_t used in this paper in Sec. 5.

Checking DNN Predictions. $\mathcal{E}_l$ is a criterion asserting the equality of $\phi[[i]].L$ and $\phi[[i']].L$. As introduced in Sec. 2.2, this work primarily focuses on DNN image classifiers. That is, $\phi[[\cdot]].L$ are image labels, and $\mathcal{E}_l$ directly checks the equivalence of two labels.

Case Study. Fig. 4 shows a case where the DNN mis-classifies a "Border Collie" image as "German Shepherd" when the original image in Fig. 4(a) is slightly blurred. We present the DNN decision D and D' in Fig. 4(b) and Fig. 4(c), respectively. As highlighted in Fig. 4(b), the DNN relies on the black `ear` and the black-and-white `neck` to decide the "Border Collie." In contrast, when Fig. 4(a) is blurred as in Fig. 4(c), the DNN instead focuses on the `tongue` and predicts the dog as "German Shepherd." An important observation, as illustrated in Sec. 6, is that *$\phi[[i]].D$ and $\phi[[i']].D$ generated using our decision-based MR_r are always different when $\phi[[i]].L \neq \phi[[i']].L$.*

Checking DNN Decisions. $\mathcal{E}_d$ is a criterion asserting the equality of $\phi[[i]].D$ and $\phi[[i']].D$. We introduce an XAI-based approach to constructing $\phi[[i]].D$, denoting the decision of DNN over i, in Sec. 4. Nevertheless, considering each decision composes a collection of image fragments (each fragment is a visual concept; see Sec. 4), asserting the *equality* is too strict because image fragments could slightly drift without undermining the DNN overall decisions. The computer vision community primarily uses the Intersection over Union (IoU) metrics to quantify two regions' overlapping. The calculation of IoU will be given in Sec. 4.2. We deem two decisions violate $\mathcal{E}_d$, in case their overlapping is smaller than a threshold T_{iou}. We empirically decide T_{iou} and present discussions in Sec. 6.2.

Case Study. We observe that several $\langle i, i' \rangle$ have zero IoU values for their decisions. Though they lead to the same prediction, this is likely due to chance. Fig. 5 shows a DNN's inconsistent decisions when its predictions are same. Fig. 5(a) is classified as "thimble" based on the highlighted `thimble` in Fig. 5(b). However, when the contrast of Fig. 5(a) is slightly lowered, the DNN still predicts "thimble" but relies on a new visual concept, the `thumb`, as depicted in Fig. 5(c). This inconsistency in DNN decisions, which was not previous detected by prediction consistency-based MT, suggests that the DNN relies incorrectly on the thumb to recognize the thimble. We deem this as a hidden defect of this DNN.

4 Forming and Comparing Decision D

We clarify the limitation of merely using pixels to form decisions in Sec. 2.4. Holistically, DNNs are designed to focus on pixel regions (e.g., using convolutional kernels [30, 31]), and each pixel should exhibit a closely correlated contribution with its neighbors. Importantly, pixel-wise contributions can be abstracted into region-wise *visual concepts*, reflecting a more holistic, robust, and human-readable view of DNN decisions. We define the decision D as the collection of all visual concepts in a test input i. We have defined visual concepts in Sec. 2.4. We present a technical solution to convert pixels (XAI outputs) to visual concepts in Sec. 4.1, and in Sec. 4.2, we compare two formed decisions D and D'.

4.1 Converting Pixels to Visual Concepts

DeepLIFT marks each pixel in an image with a contribution score. In practice, because small positive contributions (e.g., 0.001) are less informative, we denote pixels with contributions substantially higher than a threshold T_p as supporting, whereas those with lower or negative contribution scores are deemed non-supporting. That is, we binarize contributions of a pixel based on the contribution score DeepLIFT assigns to each pixel.

4.1.1 Deciding T_p The above scheme necessitates the use of a threshold T_p to decide the supporting pixels. A naïve approach may be to decide a global threshold. Nevertheless, pixel-wise contributions vary distinctly between inputs, rendering a "global threshold" less applicable. Consider the case in Fig. 3(b), where pixels of the `siren` may dominate the contributions given a "police car" image. However, `siren` may contribute less than the `cross mark` to determine an "ambulance" image. The reason is that while `cross mark` is exclusive to an ambulance, `siren` is shared by both classes.

To overcome this hurdle, our implementation adopts Otsu's method [45] to automatically decide the threshold. In brief, the Otsu's method seeks the threshold that minimizes intra-class (i.e., supporting or non-supporting) variance while simultaneously maximizing the inter-class (i.e., supporting vs. non-supporting) variance, resulting in a theoretically optimal threshold with moderate cost.

4.1.2 Joining and Detaching Supporting Pixels Using a threshold T_p decided in Sec. 4.1.1, we classify pixels into supporting vs. non-supporting ones. Then, we convert pixels into visual concepts by joining neighboring pixels that positively support the prediction and detaching isolated supporting pixels. We first introduce two elementary image processing operations, `erosion` and `dilation`, in this section. For simplicity, we represent the values of supporting and non-supporting pixels using `true` and `false`.

(a) "`zero`" image (b) after `erosion` (c) after `dilation`

Figure 6: `Erosion` and `dilation` transformations. Pixels with positive contributions are in black.

Erosion operation mimics soil erosion. As in Fig. 6(b), this operation erodes away the boundaries of positive regions. We implement `erosion` by using a kernel (similar to a 2D convolution) to slide through the image and retain a positive pixel under a kernel only if all pixels under the kernel is positive (i.e., their conjunction is positive). That is, $\texttt{erosion}(p_{k_1,k_2,\ldots,k_m}) \leftarrow \{p_{k_1} \wedge p_{k_2} \wedge, \ldots, \wedge p_{k_m}\}^m$. Dilation is the inverse of erosion. It uses a kernel to slide through the image but sets a pixel under the kernel as positive as long as any pixel under the kernel is positive (i.e., their disjunction is positive): $\texttt{dilation}(p_{k_1,k_2,\ldots,k_m}) \leftarrow \{p_{k_1} \vee p_{k_1} \vee, \ldots, \vee p_{k_m}\}^m$. As illustrated in Fig. 6(c), dilation enlarges and sharpens positive regions, which further increase their visibility.

Erosion and dilation are two common operations in image processing. They both employ a kernel to slide through an input image, resulting in an output image where the value of each pixel is determined by comparing it to its neighbors in the input image. Then,

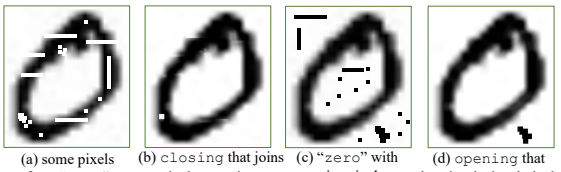

Figure 7: Closing and opening transformations.

depending on the order in which these two basic operations are used, we obtain the following two advanced operations.

Closing consists of a dilation with a subsequent erosion. That is, $\texttt{closing}(i) = \texttt{erosion} \circ \texttt{dilation}(i)$. Consider Fig. 7(a), the closing operation facilitates fill in small holes by joining supporting pixels as regions, yielding an image as in Fig. 7(b).

Opening has an erosion followed by a dilation, i.e., $\texttt{opening}(i) = \texttt{dilation} \circ \texttt{erosion}(i)$. For example, Fig. 7(c) will be converted into Fig. 7(d) after applying opening. This operation removes small, isolated supporting pixels while retaining the shape and size of large regions formed by supporting pixels. We employ this operation to remove isolated supporting pixels which may be likely induced by estimation errors of XAI.

From Supporting Pixels to Visual Concepts. To convert supporting pixels into visual concepts, we first apply closing and then opening, i.e., $\texttt{to\_concepts}(i) = \texttt{opening} \circ \texttt{closing}(i)$. The intuition is that, after joining pixels as regions, the remaining isolated pixels can be regarded as useless (or noisy) for identifying DNN decisions. The adopted operations are all standard image processing operations. These operations traverse all pixels in an image in constant time, and can be computed in parallel. $\texttt{to\_concepts}(\cdot)$ can be implemented by replacing the kernel in a 2D convolutional layer, which slides through the image and is multiplied with its covered region, with a sequence of conjunction and disjunction operations detailed in this section. 2D convolutional layers are common in image-processing DNNs. Computation cost incurred at this step is thus *equivalent to adding one DNN layer*. Moreover, the kernel size in closing and opening decides the effectiveness of extracting visual concepts: a larger kernel is more abstract and thus more robust to potential XAI errors, but less precise. We set the kernel size of closing and opening to 5 and 3, which are two most widely used kernel sizes in convolutional neuron networks that characterize the "spotting region" of common DNNs.

4.2 Measuring Inconsistent D using IoU

Our observation shows that hidden DNN defects unveiled using our MR in Eq. 1 belong to either of the following categories or their composition.

1) Missing visual concepts occurs when the tested DNN relies on a subset of the original visual concepts for prediction. As in Fig. 3, suppose the tested DNN neglects the cross mark under certain perturbations, it has to output "police car" or "ambulance" by chance according to our analysis. By checking "missing visual concepts," we unveil DNN defects even if the prediction is still "ambulance."

2) New visual concepts occurs if the tested DNN uses irrelevant visual concepts in the image to make decisions. Recall our motivating example in Fig. 1, where the DNN relies on a flower in Fig. 1(d) as a new visual concept for prediction. Such incorrect decision can also be uncovered by checking the decision consistency.

Overall, the above cases should *not* happen since we mutate test inputs using *semantics-preserving* MR_t. See MR_t adopted in this research in Sec. 5. We use IoU to measure the overlapping of decisions D and D' captured in a test input and its mutated input. The calculation of IoU is illustrated in Fig. 8. Overall, each IoU value is a number from 0 to 1 that quantifies the degree of overlapping between two regions.

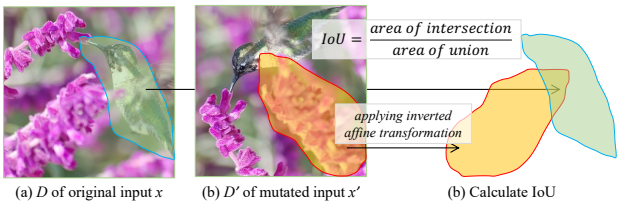

Figure 8: IoU calculation. For this case, since x' is generated by using affine transformation over x, the IoU is calculated after inverting this affine transformation on D'.

Clarification on MR. Careful readers may wonder if the above oracle is a bit too strong, because adding/missing a non-important visual concept may not affect DNN predictions from human perspectives, e.g., missing one *cross mark* may not alter predicting "ambulance" for Fig. 3. Nevertheless, besides classification, features (i.e., the outputs of intermediate layers) extracted from classifiers typically facilitate (security-sensitive) downstream tasks like object tracking and auto-driving, where adding/missing visual concepts can be more serious and likely lead to severe outcomes [16, 20, 47]. Moreover, to take into account cases where inconsistent visual concepts are valid, we employ human evaluations to decide a threshold (see **RQ2** in Sec. 6.2) to better decide visual concept "inconsistency."

Table 2: Metamorphic transformations MR_t adopted.

MR_t	**Original x ⇒ Mutated Image x'**	Used by
Pixel Level	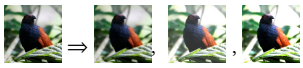	[46],[59], [64],[10]
Affine Type		[46],[59], [64],[10]
Weather Filter	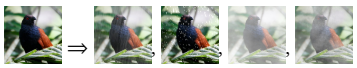	[59]
Style Transfer	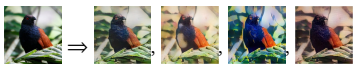	[68]
Adv. Perturb.	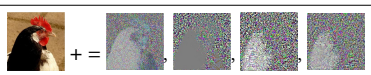	[17],[39], [4],[29]

5 Implementation & Setup

The entire codebase of this research, including scripts to form decision-based MR_r and extend prior MR_t, has about 1500 lines of Python code. We use DeepLIFT, a popular XAI framework, to flag pixel-wise contributions. We reuse and extend MR_t implementation of existing MT-based DNN testing frameworks. Most existing MT-based DNN testing works test image classification models by mutating images. MR_t in prior works are essentially semantics-preserving image mutations, as reviewed below.

Pixel-Level Mutations. This scheme contains multiple instances. By adding a same constant to all pixels of an image, we can change image brightness. Similarly, multiplying all pixels with a same constant can change image contrast. Blurring is implemented by multiplying the image with a sliding kernel. These three mutations are adopted to assess the robustness of DNNs [10, 44, 46, 59, 64].

Affine Transformations. This scheme mutates objects in images by applying invertible transformations such as translating, rotating, scaling, and shearing. These transformations preserve the collinearity of objects, thereby retaining correct semantics of objects after mutation. These methods are used to diverse images [10, 59, 64].

Clarification. Recall that our MR_r checks the consistency of decision D. Nevertheless, affine transformations, by mutating objects in an image, unavoidably change the localization of visual concepts. Thus, we calculate the IoU after inverting the applied affine transformation on generated visual concepts. For instance, if the applied affine transformations left rotate 90 degrees, we measure the IoU after first right rotating the visual concepts by 90 degrees.

Weather Filters. To simulate various weather conditions in real scenarios, weather filters, including snowy, foggy, rainy, and cloudy, are widely adopted to mutate test inputs of DNNs. We adopt weather filters proposed in [26, 59] for mutation.

Style Transfer. Style transfer was first proposed by [68], which is specifically launched to transfer (severe) weathers from a source image to a target image. The generated weather conditions in the target are usually in a higher quality than using weather filters. This approach, however, is limited to driving scenes. We extend it to general style-transfer such that arbitrary real images can be mutated. Style transfer primarily mutates image colors and retain the semantics. Our mutations include 72,521 styles; see our code [1].

Remarks. The weather filters and style transfer are only applied on CIFAR10 and ImageNet which consist of real images. Images in MNIST, a small synthetic dataset, are handwritten digits where no "weather" exists. It is also infeasible to change the color scheme via style transfer, given images in MNIST are black-and-white without the color channel (e.g., the RGB channel in real images).

Adversarial Perturbations. Guided by DNN gradients, adversarial perturbations generate adversarial examples (AEs) to fool DNNs. AEs are usually less notable or visually identical to source images. As shown in Table 2, adversarial perturbations often highlight key objects in an image. We employ four popular algorithms, FGSM [17], PGD [39], C/W [4] and BIM [29], to generate AEs.

The above mutations are frequently used in previous works: with carefully chosen parameters (i.e., to what extent the mutation is applied), they generally retain the semantics (visual consistency) in the mutated images. Therefore, a functional DNN should preserve its decisions under these mutations. In experiments, we ship MR_t configurations from previous works [10, 24, 46, 59, 64] and only mutate a seed (a real image) once; see our implementation in [1].

Table 3: Evaluated DNN models.

Model	Dataset	Remark
ResNet50 [21]	ImageNet [11]/CIFAR10 [27]	Non-sequential structure
VGG16 [55]	ImageNet/CIFAR10	Sequential structure
MobileNet-V2 [23]	ImageNet/CIFAR10	Mobile devices
DenseNet121 [25]	ImageNet	Extremely deep model
Inception-V3 [57]	ImageNet	Feature representation
LeNet1 [31]	MNIST [12]	Black-white images
LeNet5 [32]	MNIST	Black-white images

Table 4: Correctness of identified decisions. We report the percentage of unchanged outputs (left) when only keeping the decisions, and the percentage of changed outputs (right) when masking decisions in inputs.

ResNet50 ImageNet	VGG16 ImageNet	MobileNetV2 ImageNet	DenseNet121 ImageNet	Inception-V3 ImageNet
96.0%, 100%	96.8%, 100%	96.5%, 100%	96.9%, 100%	95.8%, 100%
ResNet50 CIFAR10	VGG16 CIFAR10	MobileNetV2 CIFAR10	LeNet1 MNIST	LeNet5 MNIST
97.6%, 93.8%	95.8%, 92.6%,	96.8%, 92.7%	96.2%, 91.8%	96.9%, 93.5%

Preparing Datasets $\hat{I}_=$ and $\hat{I}_\neq$. We prepare an image set I by randomly selecting images from a dataset listed in Table 3. These three datasets are the most widely-used datasets for DNN testing. For each $i \in I$, we mutate it with different $\mathtt{t} \in MR_t$, as presented in Table 2, and produce $i_\mathtt{t} = \{\mathtt{t}(i) | \mathtt{t} \in MR_t\}$.[4] Then, for each i and its mutated $i' \in i_\mathtt{t}$, we construct a set $\hat{I}$ with image pairs $\langle i, i' \rangle$, namely, $\hat{I} = \{\langle i, i' \rangle | i \in I, i' \in i_\mathtt{t}\}$. We further divide $\hat{I}$ into two collections: 1) $\hat{I}_=$ where the DNN ϕ has the same prediction label for i and i', i.e., $\hat{I}_= = \{\langle i, i' \rangle | \phi[[i]].L = \phi[[i']].L, \langle i, i' \rangle \in \hat{I}\}$, and 2) $\hat{I}_\neq$ where the DNN ϕ yields inconsistent labels for i and i', i.e., $\hat{I}_\neq = \{\langle i, i' \rangle | \phi[[i]].L \neq \phi[[i']].L, \langle i, i' \rangle \in \hat{I}\}$. For each tested DNN, we keep generating $\hat{I}$ until both $\hat{I}_=$ and $\hat{I}_\neq$ has 10,000 pairs.

Preparing Tested DNNs. We list all DNN models tested in this paper in Table 3. Note that for the first three models, we use two instances trained over two different datasets, ImageNet and CIFAR10. All ImageNet-trained models are officially provided by PyTorch and other models are well-trained (over 94% test accuracy). They are commonly used in daily DNN tasks and testings.

6 Evaluation

We primarily study the following research questions. **RQ1**: Is the identified decision D in each DNN input correct? We answer this question in Sec. 6.1. **RQ2**: Are inconsistency of decisions $D_1 \neq D_2$ truly reflect DNN defects? We launch large-scale human evaluation to explore this question from different aspects in Sec. 6.2. **RQ3**: How many and how frequent hidden defects are overlooked by existing MT-based DNN testing? What are the characteristics of these hidden defects? We answer this question in Sec. 6.3.

6.1 RQ1: Correctness of Decisions

It is challenging to assess the correctness of obtained decisions: as clarified in Sec. 2.2, we lack the ground truth decisions D_G for diverse real-world images. Furthermore, given that DNNs are designed to discover (subtle) patterns inherent in the data, it is likely that they make decisions using visual concepts that are diametrically different from human judgments, but still valid.

[4] Note that a MR_t $\mathtt{t}$ may be used for multiple times, each with a randomly selected configuration, e.g., rotation degree or brightness level.

To measure the correctness of captured decisions, we aim to construct *contradictory facts* to the DNN to assess the accuracy of decisions. Our intuition is that if and only if the identified visual concepts correctly constitute the decisions of the DNN, the DNN prediction should *not* be changed when only these visual concepts are extracted to form DNN inputs. Accordingly, if the identified visual concepts in an input are masked, the DNN prediction should change (as it loses the decisions).

For each tested DNN, *the above schemes are performed for the original inputs and the mutated input pairs from both $\hat{I}_{=}$ and $\hat{I}_{\neq}$*. Results are reported in Table 4. We also use the above masking schemes directly toward pixels identified by conventional XAI techniques, including raw outputs of DeepLIFT. For both two masking schemes, they only have around 50% of outputs unchanged/changed. In contrast, the converted visual concepts are more reliable, as it better correlates with our expectation: when identified visual concepts are masked, over $1 - \frac{1}{C}$ of outputs are changed (100% in ImageNet cases), where C is the #classes. Since the DNN has $\frac{1}{C}$ chance to guess the output, our identified decisions are precise. Similarly, when inputs only contain the identified decisions, all models have over 95% outputs unchanged. Most identified visual concepts are small fragments in images (they may be "invalid" as an input image). Thus, it is reasonable that the results are slightly lower than 100%. Overall, we interpret that decisions extracted by our technique represent the true decisions of various DNNs.

Answer to RQ1: With experiments based on contradictory facts, we illustrate the accuracy of extracted decisions. We also find that the decision, denoting regions on images, are more reliable than merely the pixels extracted by XAI.

6.2 RQ2: Human Evaluation

We now analyze how IoU values, which are derived by comparing the visual concepts of an image pair $\langle i, i' \rangle$, of $\hat{I}_{=}$ and $\hat{I}_{\neq}$, are distributed. We first report that for all image pairs in $\hat{I}_{\neq}$, the maximal IoU value $v < 0.8$, indicating that visual concepts among i and i' are *always different* whenever the DNN yields different labels. Moreover, we report that the IoU value v calculated over images in $\hat{I}_{=}$ ranges from 0 to 1. Obviously, an IoU value $v = 1$ indicates that the decisions of i and i' are exactly the same, falling into the ① case in Table 1 where $L_1 = L_2$ and $D_1 = D_2$. An IoU $v = 0$, in contrast, illustrates that the decisions in i and i' are deemed as different. For such cases, it is clear that the DNN makes an incorrect prediction, falling into scenario ③ of Table 1 where $L_1 = L_2$ and $D_1 \neq D_2$.

When the IoU value $0 < v < 1$, it is unclear if DNN makes incorrect predictions. A simple method is to consider two decisions distinct as long as $v < 1$. However, our manual analysis shows that for $\hat{I}_{=}$, $v < 1$ does not necessarily imply that the DNN makes different decisions over i and i'. For instance, the non-overlapping may be caused by different fragments on grass and clouds and other large objects in i. Despite the existence of non-overlapping visual concepts, they all represent the same object. Similarly, a relatively higher (near to 1) IoU value does not always indicate no defect, as some *small yet critical* visual concepts may cover only a small portion of areas among all identified ones (e.g., the cross mark in an ambulance; see Fig. 3).

We conduct human evaluations to explore to what extent the IoU value can reflect the inconsistency of two decisions D and D'. We form a group of 25 participants to answer a total of 10,000 questions. Given images from CIFAR10 and MNIST have relatively lower resolution, we only use images from ImageNet — the de facto real-life dataset which has the largest scale among all evaluated datasets. All evaluations are performed on the Amazon Mechanical Turk platform. We explain the setup and give quantitative results in following sections. Qualitative feedbacks are in supplementary [1].

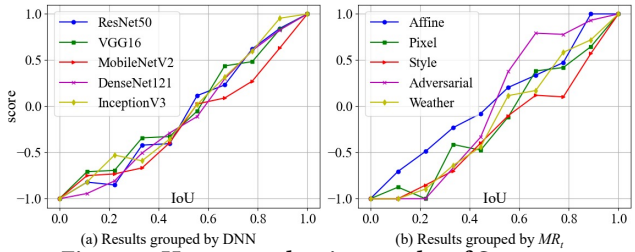

Figure 9: Human evaluation results of Sec. 6.2.1.

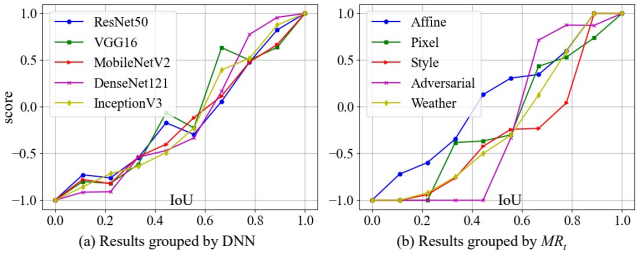

Figure 10: Human evaluation results of Sec. 6.2.2.

6.2.1 Are Decisions Same? Since understanding the visual concept and DNN decisions may be obscure for laymen, we invite 15 Ph.D. students with experience in computer vision and DNN related projects to participate this evaluation. Prior to the experiment, we teach a student what a visual concept is through examples and explain how to distinguish consistent/inconsistent DNN decisions, until the student is confident that he/she understands the prior knowledge. The teaching takes in average 30 minutes for each participant; we provide full materials used at this step to benefit future research on our released artifact [1].

We use five popular and representative DNNs trained on ImageNet, as listed in Table 3. For each model, we randomly select 500 pairs of images, which are evenly generated by each type of MR_t we introduced in Sec. 5, from $\hat{I}_{=}$ and collect a set of total 2,500 pairs. We then repeat each pair three times so that three participants can analyze each pair of decisions. The totaling 7,500 images are evenly assigned to 15 participants. Each participant may halt the human evaluation anytime to avoid fatigue. On average, each participant requires 2.5 hours to finish the entire evaluation.

For each question, we present the student three images: the original image i and two images displaying only the decisions of i and $\hat{i}$. Then, we ask whether the two decisions are equivalent (i.e., they rely on the same set of visual concepts). Students may select "`Yes`", "`No`", or "`Not sure`", which count 1, -1, 0, respectively. As aforementioned, since DNNs are designed to explore (subtle) patterns

in data, it can be difficult for humans to deduce the image content given only the visual concepts captured by DNNs. By providing the original image i, students grasp the "whole picture" in the image, and we find this helps them compare decisions in i and $\hat{i}$. Otherwise, they may just compare the pixel-wise difference, if they have no idea about what is displayed in the image.

Moreover, we find that students may fail to truly understand the requirements of this experiment, resulting in potentially invalid findings. As a common practice, we prepare and insert a number of sanity-check (SC) questions randomly into the raised questions without prior notice. Students must correctly answer SCs in order to justify the reliability of their answers. Specifically, in some questions, we present two identical decisions (i.e., extracted from the same image), for which participants should answer "yes." We also reorder the two images of decisions in some questions to generate duplicated questions — reordering makes students less likely to notice that they have already answered this question; for duplicated questions, student should answer consistently with the original questions. We discard answers from students who correctly answer $< 95\%$ SC questions. *All participants have passed the sanity check.*

To analyze the results, we group questions by 1) model and 2) the type of MR_t. We show how the scores of questions change with IoU values in Fig. 9. It is evident that each question's score has a strong positive correlation with the IoU value. When the decisions of $\langle i, i' \rangle$ have a small IoU value (< 0.2), nearly all participants agree that they denote *different* decisions. Similarly, most participants regard two decisions as the same if they have a sufficiently higher IoU value (> 0.8). From Fig. 9, we notice that in all cases (i.e., grouped by 5 models, or 5 types of MR_t), scores of $\langle i, i' \rangle$ pairs are less than 0 when the corresponding IoU values are smaller than 0.5. Moreover, the score is around -0.75, when the IoU values are smaller than 0.2. This indicates the majority of participants agree that the two decisions are different. As a practical setup, we recommend IoU values in the vicinity of 0.2.

6.2.2 How Apparent the Decisions Change? To better justify our findings, we further conduct an experiment to evaluate how apparent the decision changes are via assessing whether they are human-perceptible *at the first glance*. The intuition is that, if the difference can be noticed at the first glance, it is likely induced by distinct visual concepts and thus indicates a DNN defect. This experiment follows mostly the same setup as in Sec. 6.2.1 but only shows the decisions of i and i' *two seconds*. Moreover, to make the results more general (students with different backgrounds may have distinct preference; see their feedbacks in [1]), we invite another 10 Ph.D. and masters students with *various backgrounds* to evaluate total 2,500 pairs of decisions from $\hat{I}_{=}$; see detailed setups in [1]. We present results in Fig. 10. Compared to Fig. 9, results in Fig. 10 has a slightly higher fluctuation, which may be due to the participants' small time window (2 seconds). Nevertheless, we observe that trends in Fig. 9 and Fig. 10 are highly consistent, indicating that the decisions are *highly recognizable* and of *high quality*.

6.2.3 Agreements of Participants We use Fleiss' kappa to evaluate the reliability of our human evaluation results. The Fleiss' kappa is widely used to assess the agreement among choices of multiple (> 2) participants. A kappa value of 1 indicates that all participants totally agree on a choice, whereas kappa values ≤ 0 imply participants made completely random choices.

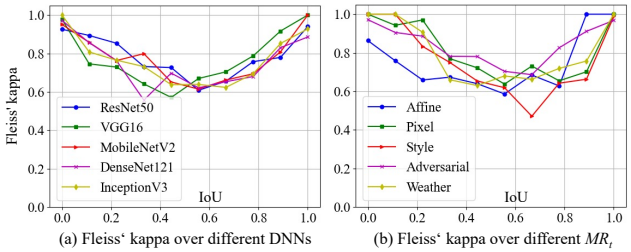

(a) Fleiss' kappa over different DNNs (b) Fleiss' kappa over different MR_t

Figure 11: Fleiss' kappa reflects the agreement of participants in Sec. 6.2.1. We report how the kappa coefficients change with the IoU of $\langle i, i' \rangle$ over different DNNs and types of MR_t. The overall Fleiss' kappa is 0.756.

The overall Fleiss' kappa coefficients for the human evaluations in Sec. 6.2.1 and Sec. 6.2.2 are 0.756 and 0.762, indicating a substantial agreement among all participants on all $\langle i, i' \rangle$ pairs [19, 54]. We further present how the kappa coefficients for various DNNs and MR_t types vary with the IoU value of decisions D and D' in Fig. 11 (for Sec. 6.2.1; see the figure for Sec. 6.2.2 in [1]). We note that the results are consistent regardless of the DNN or MR_t: when the IoU values of $\langle i, i' \rangle$'s decisions lie in $[0, 0.2] \cup [0.8, 1.0]$, the kappa coefficients of all participants are close to 1 (and in some cases reach 1); this indicates a nearly perfect agreement [19]. Overall, all participants concur that two decisions are different if their corresponding IoU score is less than 0.2. In sum, we view the Fleiss' kappa scores are aligned with our observation in Sec. 6.2.1: IoU score threshold 0.2 is generally accurate to highlight distinct decisions.

User Feedback. We present representative feedbacks from participants in [1], regarding what they rely on to compare decisions. In short, though students' comparison results are mostly *consistent*, their strategies and focuses are distinct, indicating the high quality (interpretable from multiple perspectives) of extracted decisions.

Answer to RQ2: We make several important observation at this step. 1) When DNN makes inconsistent predictions over a pair of $\langle i, i' \rangle \in \hat{I}_{\neq}$, the decision changes are consistently obvious (maximal IoU less than 0.8). 2) When DNN makes consistent predictions over $\langle i, i' \rangle \in \hat{I}_{=}$, our human evaluation illustrates that IoU values can faithfully reflect the underlying inconsistency of DNN's decisions D and D' extracted from $\langle i, i' \rangle \in \hat{I}_{=}$. Empirically, 0.2 appears to be a good threshold, such that when the IoU between D and D' is below 0.2, D and D' are deemed as different from most human's perspective.

6.3 Analysis of Hidden Defects

This section revisits existing MT-based testing frameworks through the lens of our decision-based MR_r. Fig. 12 and Fig. 13 show how IoU values, which are grouped by models or the types of MR_t over $\langle i, i' \rangle \in \hat{I}_{=}$, are distributed.

6.3.1 Results Overview We note that for each model, or each type of MR_t, almost half of the $\langle i, i' \rangle$ pairs have IoU values less than 0.5. Given that DNNs are still making "consistent" predictions over i and i', we thus deem that a large number of hidden defects are not

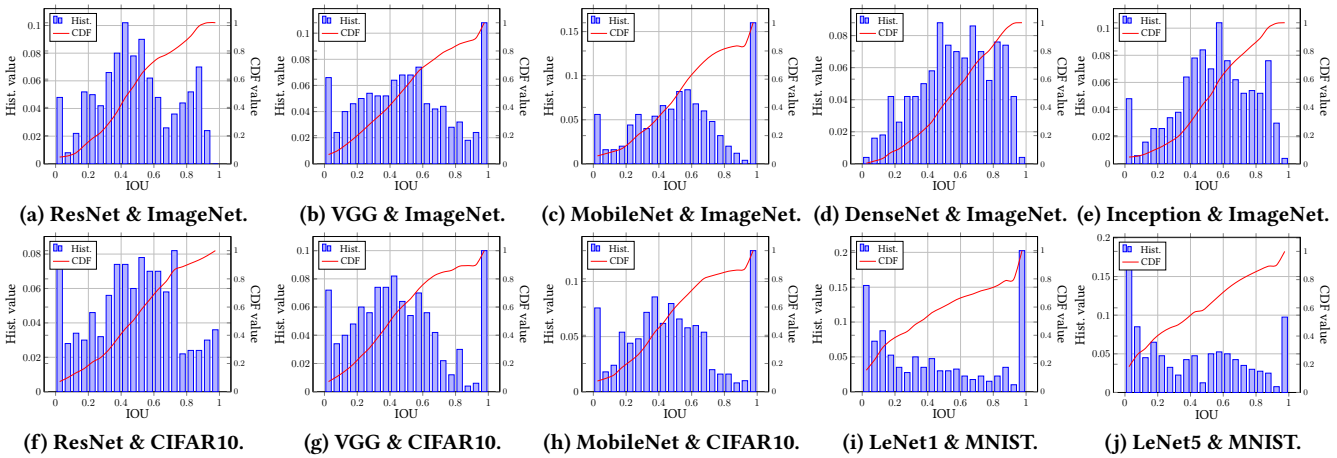

(a) ResNet & ImageNet. (b) VGG & ImageNet. (c) MobileNet & ImageNet. (d) DenseNet & ImageNet. (e) Inception & ImageNet.

(f) ResNet & CIFAR10. (g) VGG & CIFAR10. (h) MobileNet & CIFAR10. (i) LeNet1 & MNIST. (j) LeNet5 & MNIST.

Figure 12: Histograms of IoU values (grouped by DNN) over D of $\langle i, i' \rangle \in \hat{I}_{=}$. Red line denotes cumulative distribution (CDF).

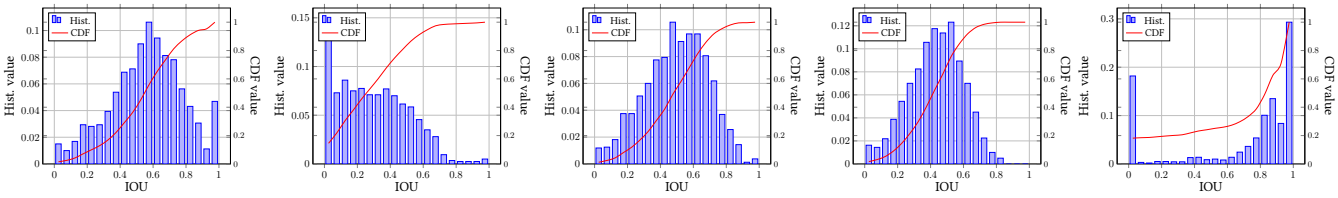

(a) Pixel-Level. (b) Affine (c) Weather Filter. (d) Style Transfer. (e) Adv. Perturbation.

Figure 13: Histograms of IoU values (grouped by MR_t) over D of $\langle i, i' \rangle \in \hat{I}_{=}$. Red line denotes cumulative distribution (CDF).

detected by existing MT frameworks merely checking DNN prediction consistency. We now analyze hidden defects' characteristics.

Comparing Different DNNs. Fig. 12 illustrates that the distributions of IoU values primarily vary in accordance with the DNN architectures (e.g., ResNet50 vs. VGG16) rather than with the training datasets (e.g., CIFAR10 vs. ImageNet). For instance, Fig. 12(a), Fig. 12(b), and Fig. 12(c) have more distinct trends, whereas Fig. 12(b) and Fig. 12(g) have correlated trends. This is an interesting observation: our evaluated DNNs are all commonly used in real-world scenarios, and they have different representative structures. Thus, it is reasonable to assume that, hidden defects due to inconsistent decisions are mostly induced by different model design. Accordingly, to fix these defects, developers are expected to focus on DNN architectures rather than simply enriching the datasets (ImageNet is much more comprehensive than CIFAR10). We present further discussions on DNN defect repairing in Sec. 7.

Comparing Different MR_t. Fig. 13 shows that IoU values corresponds to different MR_t have distinct distributions.

Adversarial Perturbations: Fig. 13(e) shows that the majority of IoU values are close to two extremes, 0 and 1. That is, the decisions of $\langle i, i' \rangle$, when their corresponding outputs are identical, are either exactly same or completely different in many cases. It also has the highest ratio of zero IoU value, indicating its high effectiveness of flipping DNN predictions. Note that adversarial perturbations are guided by DNN gradients, which are very informative for describing DNN behaviors. This can also be reflected from Table 2 where key objects in image are highlighted by adversarial perturbations. In addition, compared with other MR_t discussed below, adversarial perturbation may be more desirable, since it does not introduce much false positive/negative cases due to challenges in deciding a proper IoU threshold — as reflected from our empirical results, users may safely regard two decisions of $\langle i, i' \rangle$ as inconsistent as long as their IoU value is zero. This saves the extra effort of human assessments and confirmation.

Affine Transformations: As in Fig. 13(b), this MR_t has the highest ratio of IoU values less than 0.2, where the decisions of $\langle i, i' \rangle$ differ based on our human evaluation. It also has the second-highest ratio of zero IoU values. Recall we invert an affine transformation on decisions of i' before computing IoU. Therefore, we may infer that modern DNNs are still highly sensitive to affine transformations, which can change the position, viewing angle, size, orientation of objects, thereby introducing more diverse "patterns" in images. Compared with other MR_t (e.g., style transfer and adversarial perturbation), affine transformations manifest a relative lower cost and are applicable in most scenarios. It may be reasonable to conclude that affine transformation is a suitable pre-processing approach for generating large-scale, diverse images to better stress DNNs. Such a diverse image collection could be of high benefit in augmenting DNN training data and repairing DNNs. In fact, this strategy has been adopted by many existing works [52].

Style Transfer: As in Fig. 13(d), the highest IoU of this MR_t approaches 0.8. That is, when i is mutated into i' using style transfer,

their corresponding decisions are always distinct (in all our evaluated cases). Recent works have pointed out that DNNs trained on real datasets (e.g., ImageNet) have a texture bias: they primarily rely on texture rather than the shape of objects to make predictions. Accordingly, previous works proposed training DNNs on style-transferred images to alleviate texture-bias [15]. As shown in Table 2, style transfer changes the color schemes of an image (e.g., from realistic to artistic), which modifies the texture while retaining the object shape. Our findings illustrate the strength of style transfer, which, to a great extent, validates the motivation and argumentation of previous research. Interestingly, as demonstrated in our evaluation in Sec. 6.2, the highest IoU value calculated over decisions of $\langle i, i' \rangle \in \hat{I}_{\neq}$ is also close to 0.8. Taking Fig. 13(d) into account, we hypothesize that an IoU less than 0.8 indicates different decisions from the DNN perspective (though are less human-notable). From our empirical observation, we suggest that safety-critical DNNs (e.g., autonomous driving) employ an IoU of 0.8.

Pixel-wise Mutation & Weather Filter: Fig. 13(a) and Fig. 13(c) have similar IoU value distributions: the majority of IoU values cluster around 0.5 and values in $[0, 1]$ are all covered. Both two MR_t can be viewed as adding diverse "noise" on images. Despite being less effective than other MR_t at triggering inconsistent decisions, they still expose a number of DNN defects. Moreover, it is evident that error-triggering inputs generated by pixel-wise mutations or weather filters are distinct with those of style transfer and affine transformations, as they impose different mutation effects on images. Therefore, all MR_t proposed by prior works are demanding to stress DNNs from different angles. Also, since pixel-wise mutation and weather filter have lower cost, similar to affine transformation, it is feasible to generate large-scale, diverse image collections using these two methods. We thus believe that they are useful for augmenting DNN training data and repairing DNNs.

6.3.2 Case Study As revealed in Fig. 12, taking decision consistency into account enables detecting a large number of DNN defects from all popular DNNs. Fig. 1, Fig. 3, and Fig. 5 have shown several cases, where the decisions in the original images are largely inconsistent with the mutated images, though DNNs still (incorrectly) yields consistent labels. Due to limited space, we provide more cases at [1]: the inconsistent decisions are mostly induced by both cases that miss and add visual concepts, as described in Sec. 4.2, and they occur in images of different classes that are mutated using various methods. Overall, the diversity indicates that our decision-based oracle can find a broad set of defects. We will maintain our unveiled cases to benefit follow-up research and comparison.

Answer to RQ3: We make several key observations. 1) Decision-based MR_r unveils many DNN defects that were overlooked by existing MT frameworks. 2) When cross comparing DNNs with different architectures or trained using different datasets, we find that decision defects primarily root from the DNN architectures. Therefore, repairing the exposed defects should focus on tweaking the architectures rather than enriching the training data (further discussed in Sec. 7). 3) When cross comparing different MR_t, adversarial perturbations seem more "reliable" by omitting fewer decision defects. Nevertheless, different MR_t mutate test inputs from various angles. Their exposed defects, when taking decision consistency into account, are distinct. This illustrates the necessity of all existing MR_t.

Table 5: The number of DNN inferences within one minute on one Nvidia GeForce RTX 2080 GPU.

	ResNet50 ImageNet	ResNet50 CIFAR10	LeNet5 MNIST
Inference w/o decision	~ 6,000/min	~ 8,000/min	~ 30,000/min
Inference w/ decision	~ 1,600/min	~ 2,000/min	~ 13,000/min

7 Discussion and Future Work

Cost vs. Benefit. The extra cost of our decision-based oracle consists of ⓐ one backward propagation of DeepLIFT, and ⓑ the conversion from prediction-contributing pixels to visual concepts. As clarified in Sec. 4.1, cost of ⓑ is comparable to executing one extra DNN layer. Given that modern DNNs have tens of layers (e.g., ResNet50 has 50 layers), ⓐ introduces the majority of extra cost. We compare DNN inference speed with and without extracting decisions in Table 5: extracting decisions slows DNN inference by a factor of four. Since ⓑ has a relatively high tolerance for errors in XAI outputs (recall we abstract XAI outputs into visual concepts), the overhead can be further reduced by using various quicker (but possibly less accurate) XAI methods available off-the-shelf.

From the "benefit" perspective, we note that in Sec. 6's experiments, only about 1.5% mutated inputs result in incorrect predictions. 20 ~ 30% of the remaining 98.5% inputs (which induce consistent predictions) have IoU values smaller than 0.2 (i.e., their decisions are inconsistent), according to the cumulative distribution function (the red line) in Fig. 12 and Fig. 13. Thus, taking decision-based oracle into account would reveal many more defects than before. In sum, given the reasonable cost and the benefit, we believe it is worthwhile to integrate our new oracle into DNN testing.

Extension to Other Tasks. In this research, we primarily consider images and extract visual concepts from images to form MR_r. We clarify that our work roots the same focus as most works in this field, which test DNNs for image classification. Nevertheless, from a holistic view, our oracle asserts if DNN keeps the correct "focus" on the seed inputs and the mutated inputs; our oracle is violated if the focus is changed notably, regardless of the DNN tasks being evaluated. Thus, our oracle should be applicable to other tasks, such as activity/emotion recognition where the activity/emotion is recognized based on visual concepts.

For common image classification-based tasks, our XAI-based approach can precisely scope DNN decisions. In complex computer vision scenarios like auto-driving, classification, localization, and tracking tasks are all involved. We leave it as one future work to extend our technical pipeline to handle localization/tracking tasks. For other tasks where DNNs accept *discrete* inputs (e.g., text, tabular data, or grid), the minimal semantics-meaningful unit on these inputs is one discrete unit (similar to an image pixel), such as a word in a sentence, a cell in a table, or a dot in the grid. Testing such DNNs can be easier, as we may directly form a decision-based oracle using XAI outputs, including several critical discrete units.

Threat to Validity. This research regards the decisions of a DNN prediction as a collection of visual concepts, and evaluate the correctness of decisions by removing/keeping all visual concepts together. One threat is that some identified visual concepts are incorrect. In practice, it is challenging to assess the correctness of each visual concept individually, because removing/keeping part of the identified visual concepts may break the integrity of the decisions and lead to a different decision process.

However, we clarify that a few incorrect visual concepts, if they exist at all, should not affect our decision-based oracle for two reasons. First, DeepLIFT is a well-established XAI tool whose errors are pixel-wise, typically in the form of several inaccurately estimated contribution scores. However, instead of using the exact scores, we simply recognize pixels with positive scores. Moreover, the procedure of abstracting pixel-level contributions to visual concepts can also reduce inaccuracy. Second, we do not regard two decisions as inconsistent based solely on deviations in visual concepts. Instead, we deem decisions are "inconsistent" when their overlapping is below a small threshold. Overall, the threat of potentially incorrect XAI outputs is mostly eliminated in our implementation.

8 Conclusion

To reveal hidden DNN defects due to ill-decisions, this paper proposes to extend MT-based DNN testing by checking DNN decision consistency. Our evaluation shows that decision-based MT exhibits promising detectability for DNN defects. Our findings can provide insights for researchers that aim to launch MT toward DNNs.

References

[1] [n.d.]. Research Artifact. https://github.com/Yuanyuan-Yuan/Decision-Oracle.

[2] Marco Ancona, Cengiz Oztireli, and Markus Gross. 2019. Explaining deep neural networks with a polynomial time for shapley value approximation *(PMLR)*.

[3] Sebastian Bach, Alexander Binder, Grégoire Montavon, Frederick Klauschen, Klaus-Robert Müller, and Wojciech Samek. 2015. On pixel-wise explanations for non-linear classifier decisions by layer-wise relevance propagation. *PloS one* 10, 7 (2015), e0130140.

[4] Nicholas Carlini and David Wagner. 2017. Towards evaluating the robustness of neural networks *(IEEE SP)*.

[5] Shan Carter, Zan Armstrong, Ludwig Schubert, Ian Johnson, and Chris Olah. 2019. Exploring neural networks with activation atlases. *Distill* 1 (2019), 2.

[6] Aditya Chattopadhay, Anirban Sarkar, Prantik Howlader, and Vineeth N Balasubramanian. 2018. Grad-cam++: Generalized gradient-based visual explanations for deep convolutional networks *(WACV)*.

[7] Tsong Y Chen, Shing C Cheung, and Shiu Ming Yiu. 1998. *Metamorphic testing: a new approach for generating next test cases.* Technical Report. Technical Report HKUST-CS98-01, Department of Computer Science, Hong Kong ....

[8] Ian Covert and Su-In Lee. 2021. Improving KernelSHAP: Practical Shapley value estimation using linear regression *(ICAIS)*.

[9] Anupam Datta, Shayak Sen, and Yair Zick. 2016. Algorithmic transparency via quantitative input influence: Theory and experiments with learning systems. In *IEEE SP*.

[10] Samet Demir, Hasan Ferit Eniser, and Alper Sen. 2019. DeepSmartFuzzer: Reward Guided Test Generation For Deep Learning. *arXiv preprint arXiv:1911.10621* (2019).

[11] J. Deng, W. Dong, R. Socher, L.-J. Li, K. Li, and L. Fei-Fei. 2009. ImageNet: A Large-Scale Hierarchical Image Database. In *CVPR09*.

[12] Li Deng. 2012. The mnist database of handwritten digit images for machine learning research [best of the web]. *IEEE Signal Processing Magazine* (2012).

[13] Anurag Dwarakanath, Manish Ahuja, Sanjay Podder, Silja Vinu, Arijit Naskar, and MV Koushik. 2019. Metamorphic testing of a deep learning based forecaster. In *MET*.

[14] Anurag Dwarakanath, Manish Ahuja, Samarth Sikand, Raghotham M. Rao, R. P. Jagadeesh Chandra Bose, Neville Dubash, and Sanjay Podder. 2018. Identifying Implementation Bugs in Machine Learning Based Image Classifiers Using Metamorphic Testing. In *ISSTA*.

[15] Robert Geirhos, Patricia Rubisch, Claudio Michaelis, Matthias Bethge, Felix A Wichmann, and Wieland Brendel. 2018. ImageNet-trained CNNs are biased towards texture; increasing shape bias improves accuracy and robustness. *arXiv preprint arXiv:1811.12231* (2018).

[16] Ross Girshick. 2015. Fast r-cnn. In *Proceedings of the IEEE international conference on computer vision*. 1440–1448.

[17] Ian J Goodfellow, Jonathon Shlens, and Christian Szegedy. 2015. Explaining and harnessing adversarial examples. In *ICLR*.

[18] David Gunning, Mark Stefik, Jaesik Choi, Timothy Miller, Simone Stumpf, and Guang-Zhong Yang. 2019. XAI—Explainable artificial intelligence. *Science Robotics* 4, 37 (2019), eaay7120.

[19] Kilem L Gwet. 2014. *Handbook of inter-rater reliability: The definitive guide to measuring the extent of agreement among raters.* Advanced Analytics, LLC.

[20] Kaiming He, Georgia Gkioxari, Piotr Dollár, and Ross Girshick. 2017. Mask R-CNN. In *CVPR*. 2961–2969.

[21] Kaiming He, Xiangyu Zhang, Shaoqing Ren, and Jian Sun. 2016. Deep residual learning for image recognition. In *CVPR*. 770–778.

[22] Matthias Hein, Maksym Andriushchenko, and Julian Bitterwolf. 2019. Why relu networks yield high-confidence predictions far away from the training data and how to mitigate the problem. In *CVPR*.

[23] Andrew G Howard, Menglong Zhu, Bo Chen, Dmitry Kalenichenko, Weijun Wang, Tobias Weyand, Marco Andreetto, and Hartwig Adam. 2017. Mobilenets: Efficient convolutional neural networks for mobile vision applications. *arXiv preprint arXiv:1704.04861* (2017).

[24] Boyue Caroline Hu, Lina Marsso, Krzysztof Czarnecki, Rick Salay, Huakun Shen, and Marsha Chechik. 2022. If a Human Can See It, So Should Your System: Reliability Requirements for Machine Vision Components. *arXiv preprint arXiv:2202.03930* (2022).

[25] Gao Huang, Zhuang Liu, Laurens Van Der Maaten, and Kilian Q Weinberger. 2017. Densely connected convolutional networks. In *CVPR*.

[26] Alexander B. Jung, Kentaro Wada, Jon Crall, Satoshi Tanaka, Jake Graving, Christoph Reinders, Sarthak Yadav, Joy Banerjee, Gábor Vecsei, Adam Kraft, Zheng Rui, Jirka Borovec, Christian Vallentin, Semen Zhydenko, Kilian Pfeiffer, Ben Cook, Ismael Fernández, François-Michel De Rainville, Chi-Hung Weng, Abner Ayala-Acevedo, Raphael Meudec, Matias Laporte, et al. 2020. imgaug. https://github.com/aleju/imgaug. Online; accessed 01-Feb-2020.

[27] Alex Krizhevsky, Geoffrey Hinton, et al. 2009. Learning multiple layers of features from tiny images. (2009).

[28] HL Kundel and CF Nodine. 1983. A visual concept shapes image perception. *Radiology* 146, 2 (1983), 363–368.

[29] Alexey Kurakin, Ian Goodfellow, and Samy Bengio. 2016. Adversarial examples in the physical world. *arXiv preprint arXiv:1607.02533* (2016).

[30] Yann LeCun, Bernhard Boser, John Denker, Donnie Henderson, Richard Howard, Wayne Hubbard, and Lawrence Jackel. 1989. Handwritten digit recognition with a back-propagation network. *NIPS* (1989).

[31] Yann LeCun, Bernhard Boser, John S Denker, Donnie Henderson, Richard E Howard, Wayne Hubbard, and Lawrence D Jackel. 1989. Backpropagation applied to handwritten zip code recognition. *Neural computation* 1, 4 (1989), 541–551.

[32] Yann LeCun, Léon Bottou, Yoshua Bengio, and Patrick Haffner. 1998. Gradient-based learning applied to document recognition. *Proc. IEEE* 86, 11 (1998), 2278–2324.

[33] Zongjie Li, Chaozheng Wang, Zhibo Liu, Haoxuan Wang, Shuai Wang, and Cuiyun Gao. 2022. CCTEST: Testing and Repairing Code Completion Systems. *arXiv preprint arXiv:2208.08289* (2022).

[34] Pantelis Linardatos, Vasilis Papastefanopoulos, and Sotiris Kotsiantis. 2020. Explainable ai: A review of machine learning interpretability methods. *Entropy* 23, 1 (2020), 18.

[35] Scott M Lundberg and Su-In Lee. 2017. A unified approach to interpreting model predictions. *Advances in neural information processing systems* 30 (2017).

[36] Lei Ma, Fuyuan Zhang, Jiyuan Sun, Minhui Xue, Bo Li, Felix Juefei-Xu, Chao Xie, Li Li, Yang Liu, Jianjun Zhao, et al. 2018. Deepmutation: Mutation testing of deep learning systems. In *ISSRE*.

[37] Pingchuan Ma and Shuai Wang. 2021. MT-teql: evaluating and augmenting neural NLIDB on real-world linguistic and schema variations. (2021).

[38] Pingchuan Ma, Shuai Wang, and Jin Liu. 2020. Metamorphic Testing and Certified Mitigation of Fairness Violations in NLP Models. In *IJCAI*. 458–465.

[39] Aleksander Madry, Aleksandar Makelov, Ludwig Schmidt, Dimitris Tsipras, and Adrian Vladu. 2017. Towards deep learning models resistant to adversarial attacks. *arXiv preprint arXiv:1706.06083* (2017).

[40] Junhua Mao, Xu Wei, Yi Yang, Jiang Wang, Zhiheng Huang, and Alan L Yuille. 2015. Learning like a child: Fast novel visual concept learning from sentence descriptions of images. In *ICCV*.

[41] Grégoire Montavon, Alexander Binder, Sebastian Lapuschkin, Wojciech Samek, and Klaus-Robert Müller. 2019. Layer-wise relevance propagation: an overview. *Explainable AI: interpreting, explaining and visualizing deep learning* (2019).

[42] Shin Nakajima and Tsong Yueh Chen. 2019. Generating biased dataset for metamorphic testing of machine learning programs. In *IFIP-ICTSS*.

[43] Anh Nguyen, Jason Yosinski, and Jeff Clune. 2015. Deep neural networks are easily fooled: High confidence predictions for unrecognizable images. In *Proceedings of the IEEE conference on computer vision and pattern recognition*. 427–436.

[44] Augustus Odena and Ian Goodfellow. 2018. Tensorfuzz: Debugging neural networks with coverage-guided fuzzing. *arXiv preprint arXiv:1807.10875* (2018).

[45] Nobuyuki Otsu. 1979. A threshold selection method from gray-level histograms. *IEEE transactions on systems, man, and cybernetics* 9, 1 (1979), 62–66.

[46] Kexin Pei, Yinzhi Cao, Junfeng Yang, and Suman Jana. 2017. DeepXplore: Automated Whitebox Testing of Deep Learning Systems *(SOSP '17)*.

[47] Shaoqing Ren, Kaiming He, Ross Girshick, and Jian Sun. 2015. Faster r-cnn: Towards real-time object detection with region proposal networks. In *Advances in neural information processing systems*. 91–99.

[48] Marco Tulio Ribeiro, Sameer Singh, and Carlos Guestrin. 2016. " Why should i trust you?" Explaining the predictions of any classifier. In *KDD*.

[49] Sergio Segura, Gordon Fraser, Ana B Sanchez, and Antonio Ruiz-Cortés. 2016. A survey on metamorphic testing. *IEEE TSE* (2016).

[50] Ramprasaath R Selvaraju, Michael Cogswell, Abhishek Das, Ramakrishna Vedantam, Devi Parikh, and Dhruv Batra. 2017. Grad-cam: Visual explanations from deep networks via gradient-based localization. In *ICCV*.

[51] Lloyd S Shapley. 2016. *A value for n-person games*. Princeton University Press.

[52] Connor Shorten and Taghi M Khoshgoftaar. 2019. A survey on image data augmentation for deep learning. *Journal of big data* 6, 1 (2019), 1–48.

[53] Avanti Shrikumar, Peyton Greenside, and Anshul Kundaje. 2017. Learning important features through propagating activation differences. In *ICML*.

[54] Julius Sim and Chris C Wright. 2005. The kappa statistic in reliability studies: use, interpretation, and sample size requirements. *Physical therapy* (2005).

[55] Karen Simonyan and Andrew Zisserman. 2014. Very deep convolutional networks for large-scale image recognition. *arXiv preprint arXiv:1409.1556* (2014).

[56] Mukund Sundararajan, Ankur Taly, and Qiqi Yan. 2017. Axiomatic attribution for deep networks. In *ICML*.

[57] Christian Szegedy, Vincent Vanhoucke, Sergey Ioffe, Jon Shlens, and Zbigniew Wojna. 2016. Rethinking the inception architecture for computer vision. In *CVPR*.

[58] Yongqiang Tian, Shiqing Ma, Ming Wen, Yepang Liu, Shing-Chi Cheung, and Xiangyu Zhang. 2021. To what extent do DNN-based image classification models make unreliable inferences? *Empirical Software Engineering* 26, 5 (2021), 1–40.

[59] Yuchi Tian, Kexin Pei, Suman Jana, and Baishakhi Ray. 2018. DeepTest: Automated Testing of Deep-neural-network-driven Autonomous Cars *(ICSE '18)*.

[60] Koen EA Van de Sande, Theo Gevers, and Cees GM Snoek. 2008. A comparison of color features for visual concept classification. In *Proceedings of the 2008 international conference on Content-based image and video retrieval*. 141–150.

[61] Huiyan Wang, Jingwei Xu, Chang Xu, Xiaoxing Ma, and Jian Lu. 2020. Dissector: Input validation for deep learning applications by layer dissection *(ICSE)*.

[62] Shuai Wang and Zhendong Su. 2020. Metamorphic Object Insertion for Testing Object Detection Systems. In *ASE*.

[63] Dongwei Xiao, Zhibo Liu, Yuanyuan Yuan, Qi Pang, and Shuai Wang. 2022. Metamorphic Testing of Deep Learning Compilers. (2022).

[64] Xiaofei Xie, Lei Ma, Felix Juefei-Xu, Hongxu Chen, Minhui Xue, Bo Li, Yang Liu, Jianjun Zhao, Jianxiong Yin, and Simon See. 2018. Coverage-guided fuzzing for deep neural networks. *arXiv preprint arXiv:1809.01266* (2018).

[65] Yuanyuan Yuan, Qi Pang, and Shuai Wang. 2021. Enhancing Deep Neural Networks Testing by Traversing Data Manifold. *arXiv preprint arXiv:2112.01956* (2021).

[66] Yuanyuan Yuan, Shuai Wang, Mingyue Jiang, and Tsong Yueh Chen. 2021. Perception Matters: Detecting Perception Failures of VQA Models Using Metamorphic Testing. In *CVPR*.

[67] Jie M Zhang, Mark Harman, Lei Ma, and Yang Liu. 2020. Machine learning testing: Survey, landscapes and horizons. *TSE* (2020).

[68] Mengshi Zhang, Yuqun Zhang, Lingming Zhang, Cong Liu, and Sarfraz Khurshid. 2018. DeepRoad: GAN-based Metamorphic Testing and Input Validation Framework for Autonomous Driving Systems. In *ASE*.